bears a close resemblance to the macro length scale for isotropic turbulence, but this is solely due to its definition in (4-7). The similarity of the spectral curves suggest that there exists some form of local equilibrium in the flow, i.e. between viscous dissipation and production. Also plotted on Figures 34 to 37 are the $-\frac{5}{3}$ slope of Kolmogorov and the -7 slope of Heisenberg. At the higher frequencies the -7 power law fits the spectral distributions reasonably well suggesting that at these frequencies the energy dissipation is mainly due to viscosity.

d) Criterion for Reverse Transition

The criteria proposed by Moller (1963) and Kreith (1965) were invalidated by the experiments of Bakke and Kreith (1969) on the basis that there were still turbulent fluctuations present in the flow. Unfortunately Bakke and Kreith (1969) failed to ascertain whether these turbulent fluctuations were in a state of decay or not. If the turbulent fluctuations were in a state of decay the flow would have eventually reached a laminar state at some critical radius. From Figure 29 we see that this critical radius will depend on the rate of decay. Therefore if a critical radius for laminar flow is to be formulated some dependence on the rate of decay must be incorporated into the criterion. At this stage insufficient evidence is available to formulate such a criterion but it is possible by inspecting the radial pressure distribution to determine whether the flow has reverted to the laminar state. This assertion is readily explained by looking at the equations of motion for turbulent flow between parallel disks, namely

$$U\frac{\partial U}{\partial r} + V\frac{\partial U}{\partial z} + \frac{1}{r}\frac{\partial}{\partial r}(r\overline{u^2}) + \frac{\partial}{\partial z}(\overline{uv}) = -\frac{1}{\rho}\frac{\partial P}{\partial r}$$

$$+ \nu\left\{\frac{\partial^2 U}{\partial r^2} + \frac{1}{r}\frac{\partial U}{r} - \frac{U}{r^2} + \frac{\partial^2 U}{\partial z^2}\right\} \tag{4-8}$$

$$\rho\overline{v^2} + \underline{P} = \text{constant} \tag{4-9}$$

The inertia terms in the above equation will be negligible only if the fluctuating components are smaller than the mean components, that is to say it is highly unlikely that $\overline{u^2}$ and $\overline{uv}$ will be significant when UV and U^2 are negligible. Thus when the flow has a negative pressure gradient we can be assured that the turbulent fluctuations have died out. In this study the pressure distributions depicted in Figure 22 all have a positive pressure gradient indicating that the inertia terms are still significant. From the laminar theory the negative pressure gradient will apply when

$$\frac{Re}{\hat{r}^2} << 1,$$

but as mentioned earlier it will also depend on the rate of decay of the turbulence. Thus to achieve this situation in practice a very narrow gap width as well as a low Re is required. In this study the gap width had to be sufficiently large to facilitate hot-wire measurements and therefore to achieve a situation where

$$\frac{Re}{\hat{r}^2} << 1$$

would mean having large diameter disks and consequently very low flow rates, therefore it was impossible to verify the negative pressure gradient hypothesis. Unfortunately, neither Bakke (1969) nor Moller (1963) have reported a turbulent flow having an inversion in pressure gradient. Bayley and Owen (1969) have reported such an inversion but did not determine whether the flow was in a state of decay or not.

Another criterion that is possible to formulate at this stage is when will a turbulent field begin to decay.

As shown in Figures 23 to 28 the turbulent field will either decay or else increase in intensity depending on the Reynolds number as well as the radial co-ordinate. This means that any critical Reynolds number theory for the decay of turbulence must be based on a radial, as well as a transverse co-ordinate. A Reynolds number that turns out to be suitable is

$$\hat{Re} = \frac{Re}{\hat{r}^2} \tag{4-10}$$

This is a reduced Reynolds number and for laminar flow it is just the ratio of inertia to viscous forces. From the results shown in Figures 23 to 28 decay appears to occur around $\hat{Re} \approx 8$.

The only other existing experimental results showing a decay of turbulent fluctuations between parallel disks can be found in Bakke's (1969) thesis, Fig. 18. The reduced Reynolds number for Bakke's results is 5,5 which agrees reasonably well with ours.

It is interesting to note that Kreith's (1965) criterion

$$\frac{r_c}{h} = k\left(\frac{Q}{\nu h}\right)^{1/2} \qquad (4\text{-}11)$$

which is based on the laminar theory of Peube (1963) can be rearranged to give

$$\hat{Re} = \frac{1}{4k^2} \qquad (4\text{-}12)$$

Kreith (1965) suggested that reverse transition would occur when k was approximately 0,28 which makes $\hat{Re} \approx 3{,}3$. Unfortunately, Kreith (1965) did not mention whether the turbulence was in a state of decay or whether the flow was laminar. In any event his criterion now appears to be reasonably accurate for describing the initial decay of the turbulent fluctuations.

FIGURES 16-21

Distribution of U across the channel at various radial positions and Reynolds numbers.

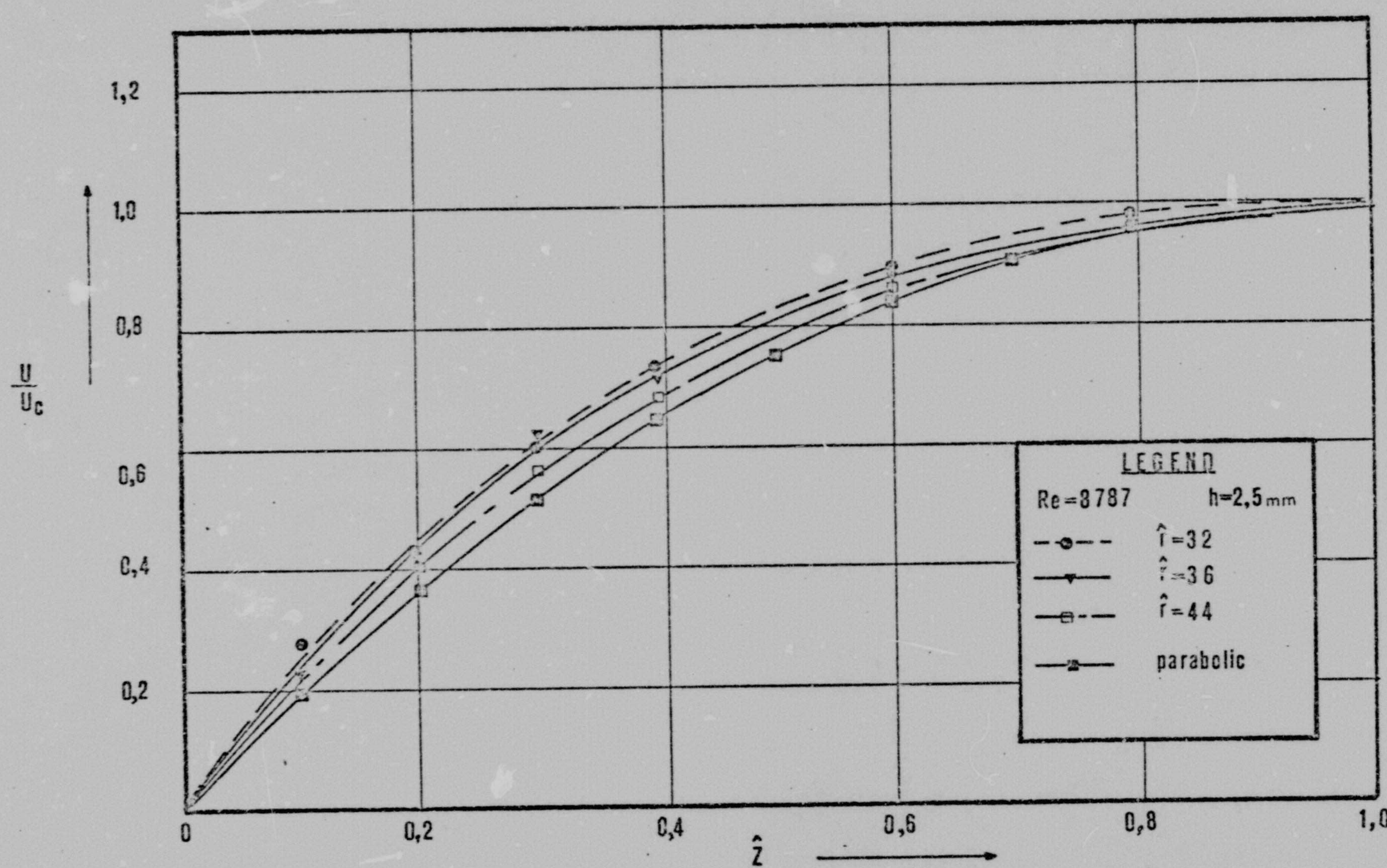
LEGEND
Re=8787
h=2,5 mm
r̂=32
r̂=36
r̂=44
parabolic
1,2
1,0
0,8
0,6
0,4
0,2
0
0,2
0,4
0,6
0,8
1,0
U/Uc
ẑ

Figure 16

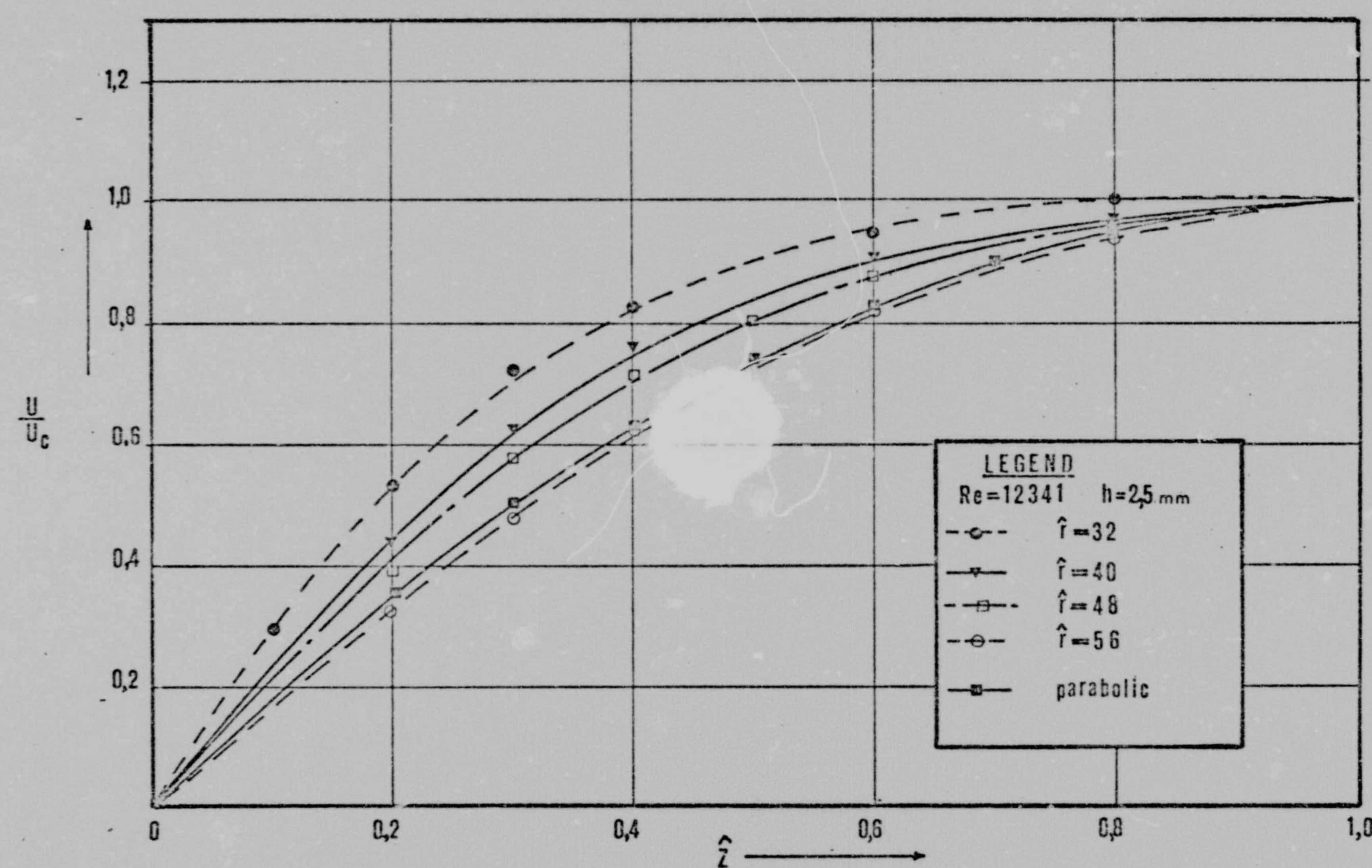
1,2
1,0
0,8
0,6
0,4
0,2
0
0,2
0,4
0,6
0,8
1,0
$\frac{U}{U_c}$
$\hat{z}$
LEGEND
Re=12341 h=2,5 mm
$\hat{r}$ = 32
$\hat{r}$ = 40
$\hat{r}$ = 48
$\hat{r}$ = 56
parabolic

Figure 17

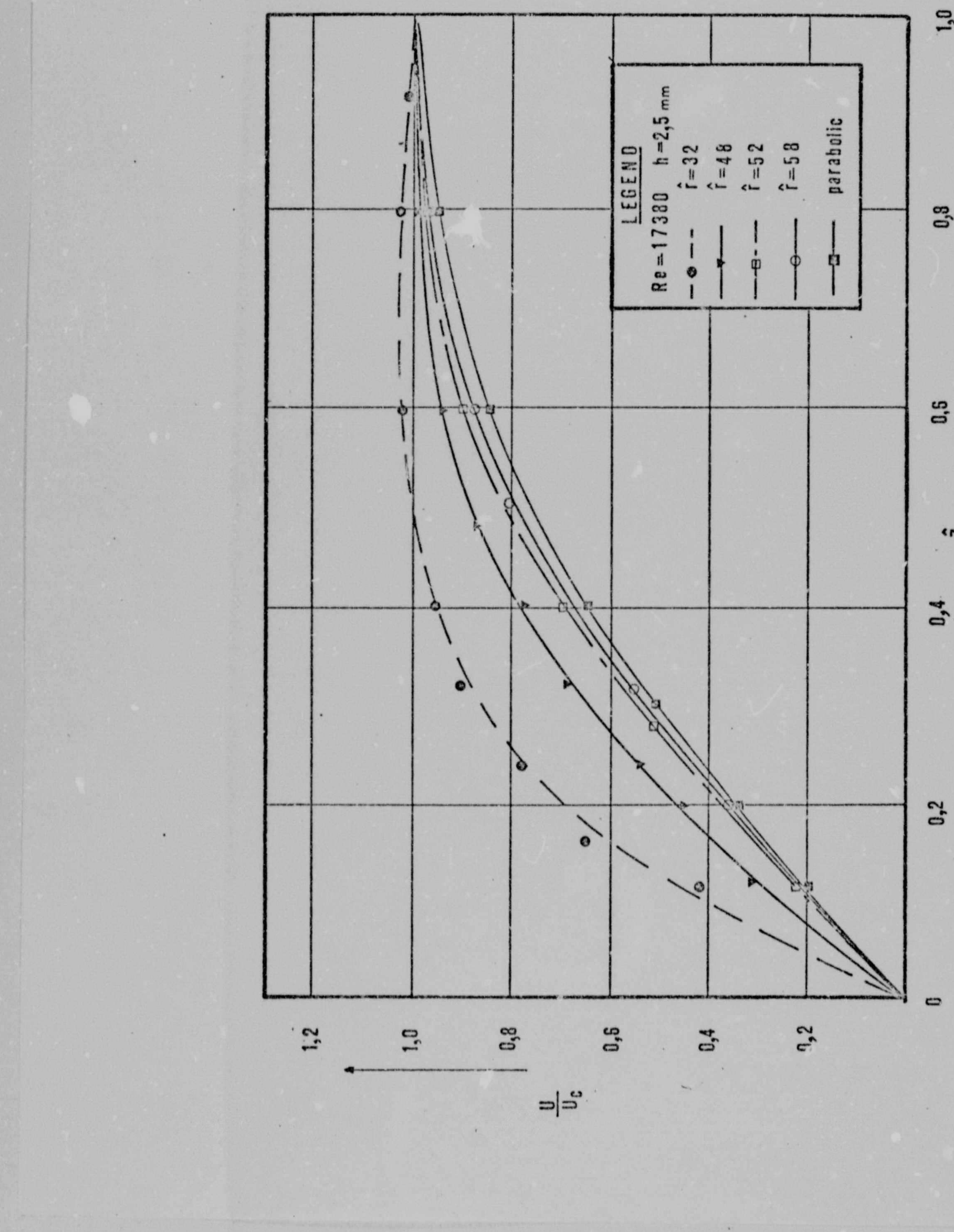
LEGEND
Re = 17380 h = 2,5 mm
$\hat{r}$ = 32
$\hat{r}$ = 48
$\hat{r}$ = 52
$\hat{r}$ = 58
parabolic
$\frac{U}{U_c}$
1,2
1,0
0,8
0,6
0,4
0,2
0
0,2
0,4
0,5
0,8
1,0
$\hat{Z}$

Figure 18

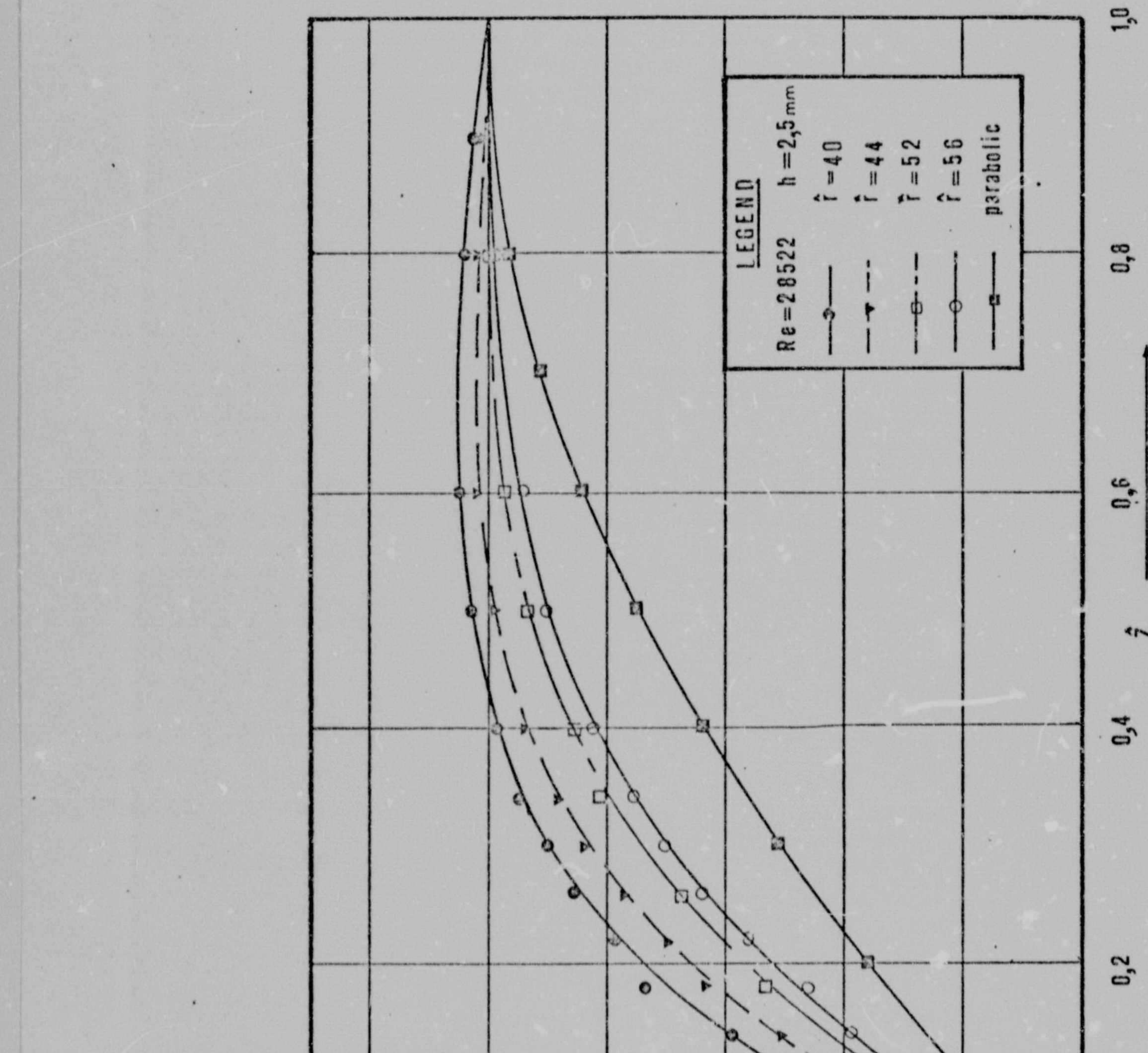
LEGEND
Re = 28522   h = 2,5 mm
r̂ = 40
r̂ = 44
r̂ = 52
r̂ = 56
parabolic
$\frac{U}{U_c}$
1,2
1,0
0,8
0,6
0,4
0,2
0
0,2
0,4
0,6
0,8
1,0
ẑ

Figure 19

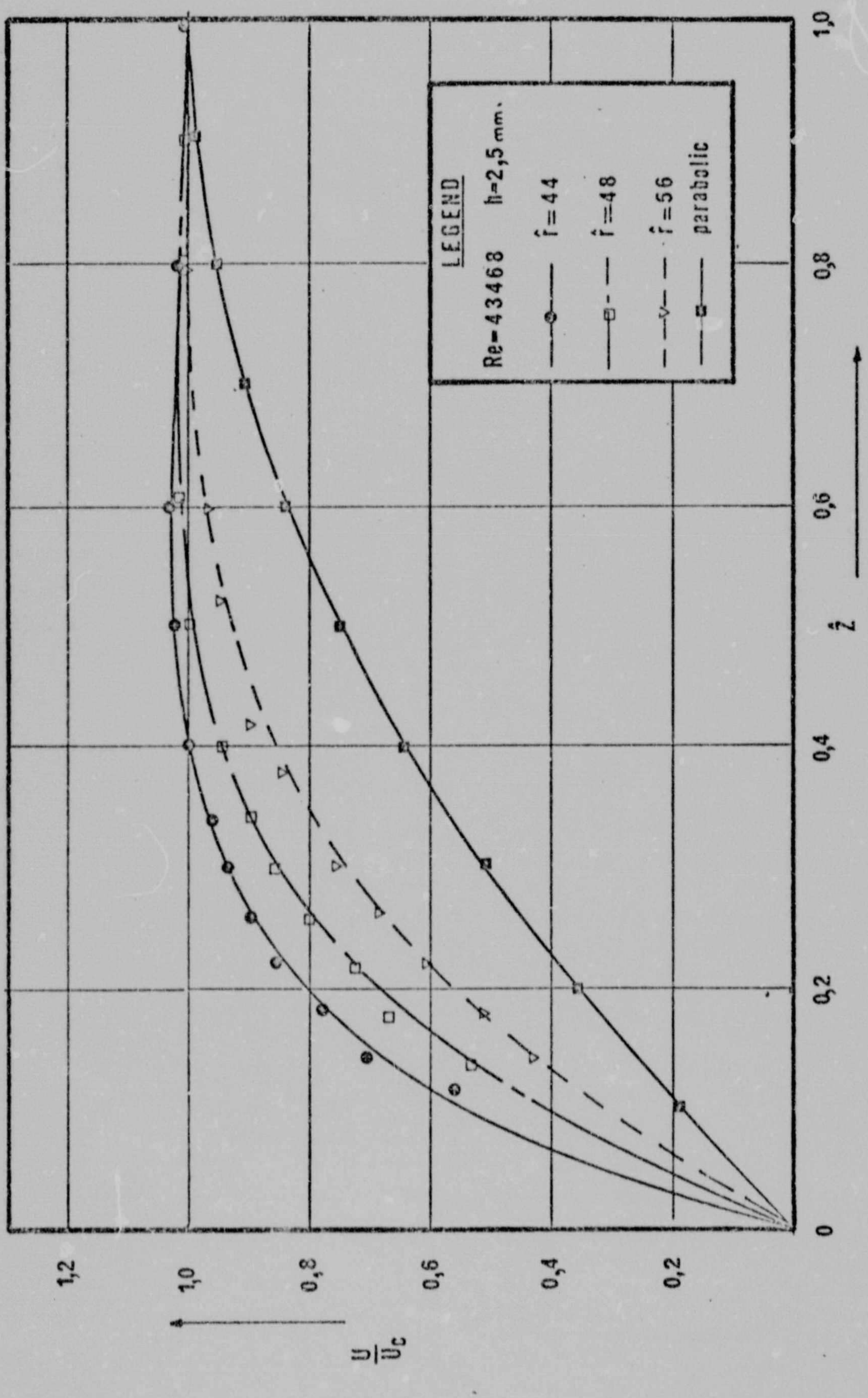

LEGEND
Re=43468 h=2,5 mm.
$\hat{f}$=44
$\hat{f}$=48
$\hat{f}$=56
parabolic
$\frac{U}{U_c}$
1,2
1,0
0,8
0,6
0,4
0,2
0
0,2
0,4
0,6
0,8
1,0
$\hat{z}$

Figure 20

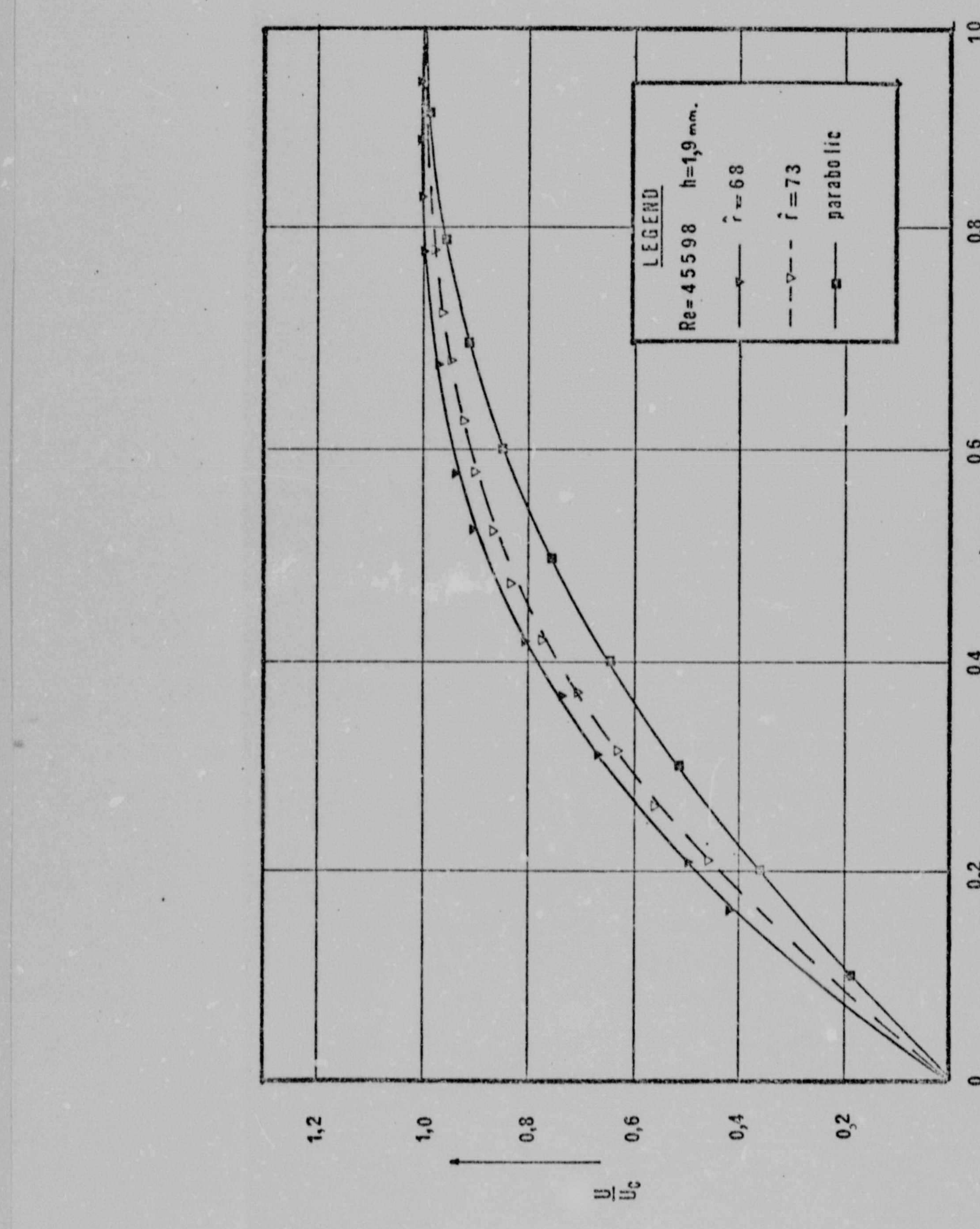
LEGEND
Re=45598 h=1,9 mm.
$\hat{r}$=68
$\hat{r}$=73
parabolic
1,2
1,0
0,8
0,6
0,4
0,2
$\frac{U}{U_c}$
0
0,2
0,4
0,8
1,0
$\hat{z}$

Figure 21

FIGURE 22

Radial pressure distributions for various Reynolds numbers.

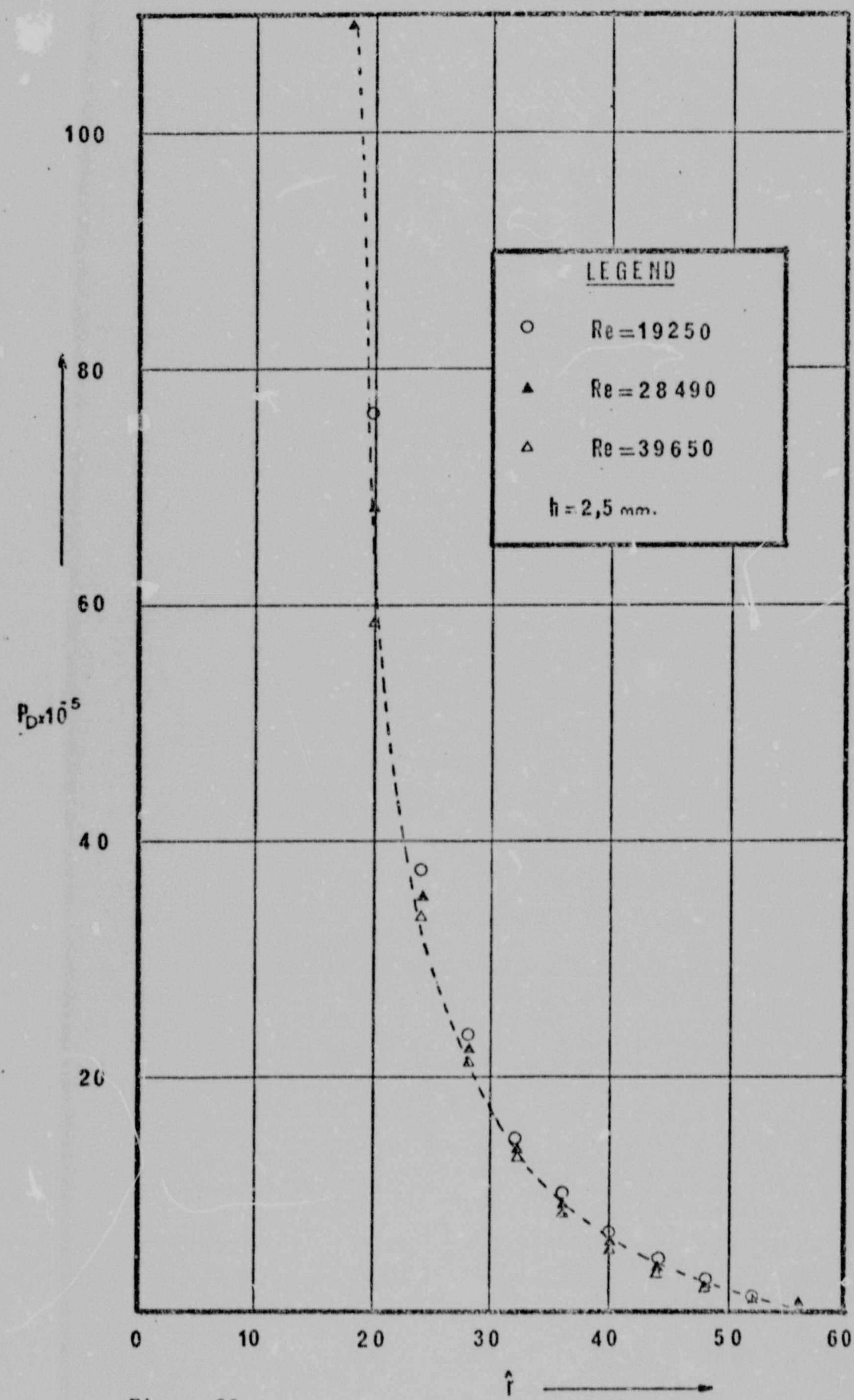
100
80
60
40
20
$P_D \times 10^{-5}$
0
10
20
30
40
50
60
$\hat{r}$
LEGEND
Re = 19250
Re = 28490
Re = 39650
h = 2,5 mm.

Figure 22

FIGURES 23-28

Distribution of $\sqrt{\frac{\overline{u^2}}{U_c}}$ across the channel at various radial positions and Reynolds numbers.

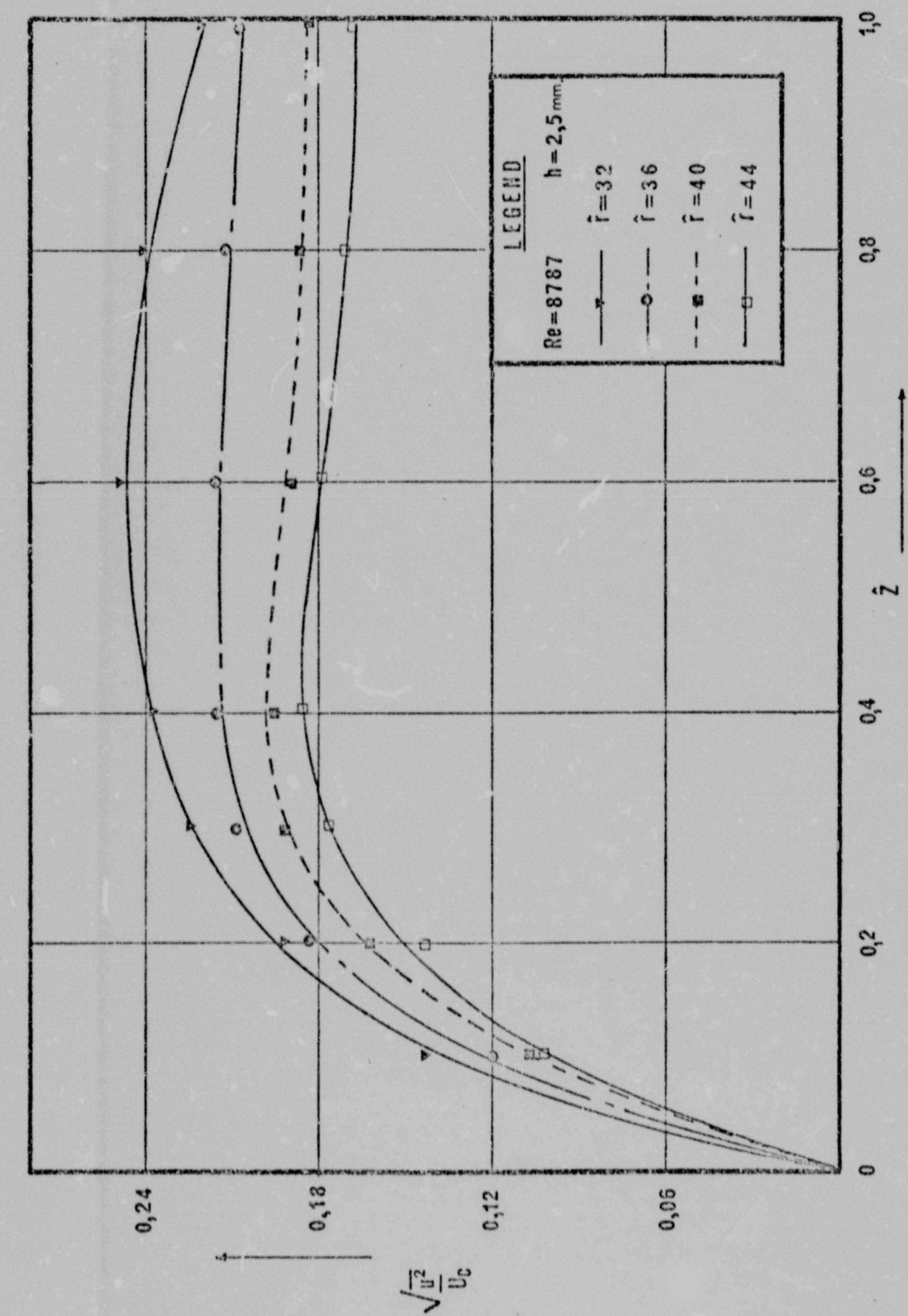
LEGEND
Re = 8787
h = 2,5 mm
r̂ = 32
r̂ = 36
r̂ = 40
r̂ = 44
0,24
0,18
0,12
0,06
$\sqrt{\overline{u'^2}}/U_c$
0
0,2
0,4
0,6
0,8
1,0
Ẑ

Figure 23

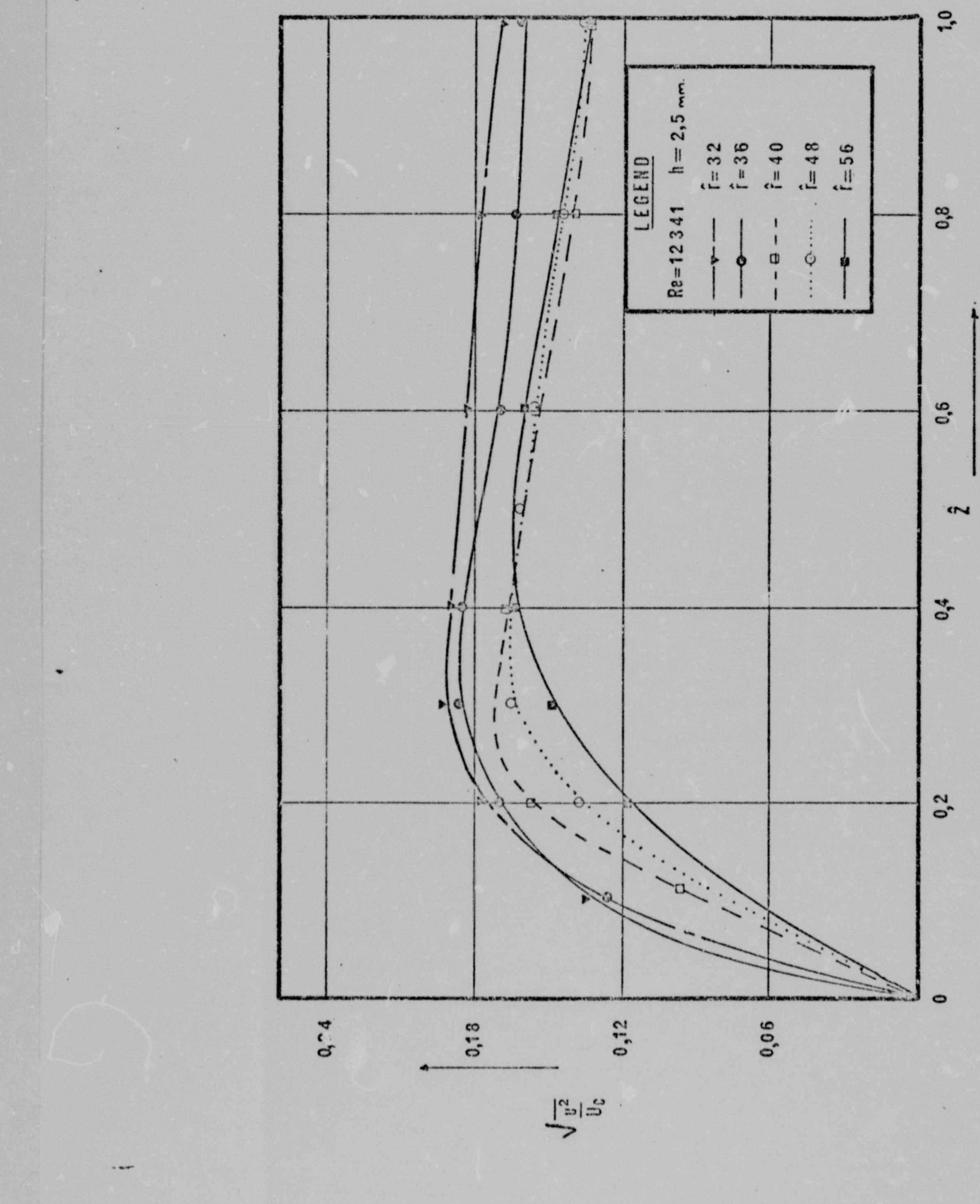
LEGEND
Re=12 341 h = 2,5 mm
r̂ = 32
r̂ = 36
r̂ = 40
r̂ = 48
r̂ = 56
0,24
0,18
0,12
0,06
0
0,2
0,4
0,6
0,8
1,0
ẑ
$\sqrt{\overline{v^2}}/U_c$

Figure 24

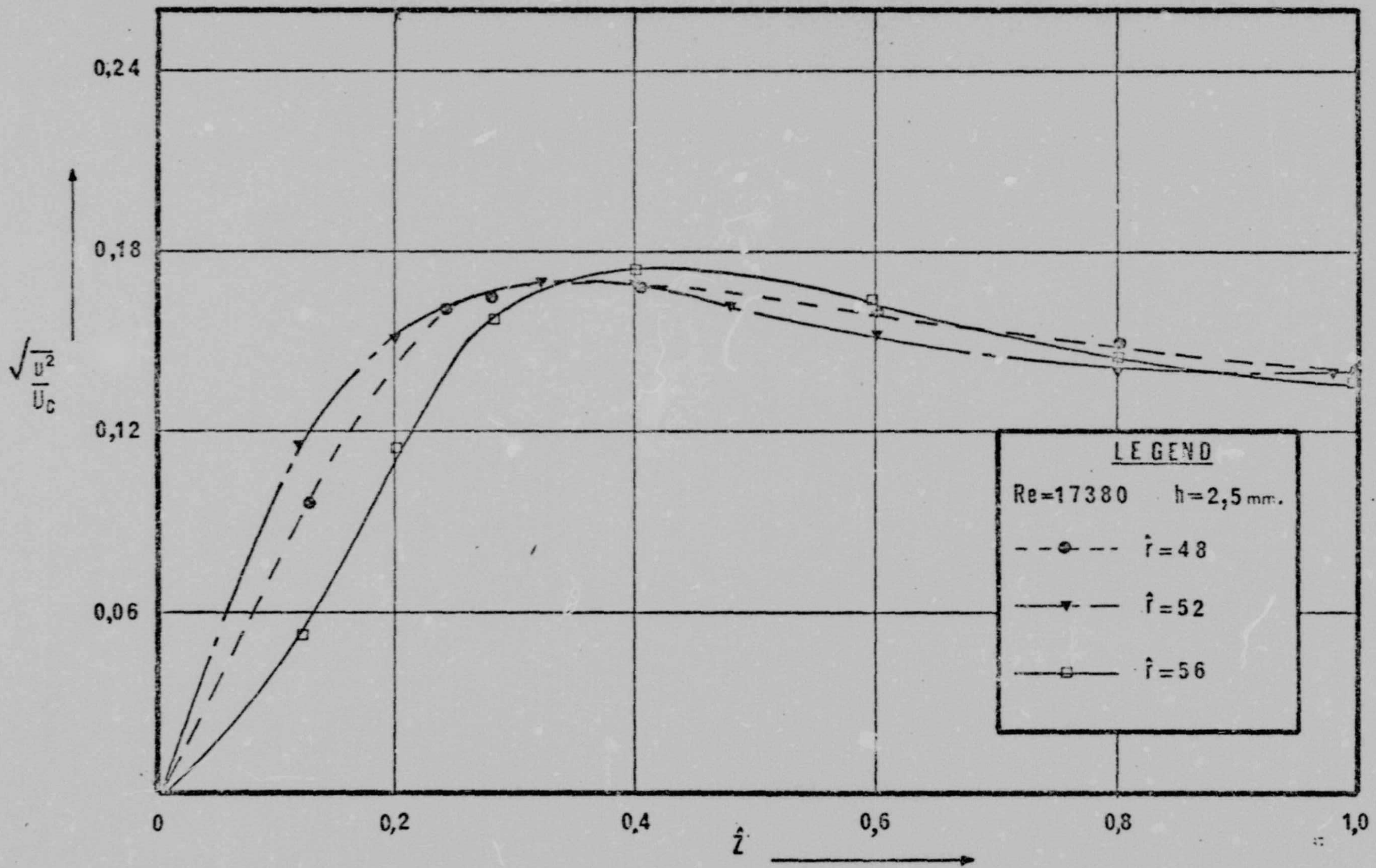
0,24
0,18
0,12
0,06
0
0,2
0,4
0,6
0,8
1,0
$\sqrt{\overline{u^2}} / U_c$
$\hat{Z}$
LEGEND
Re=17380 h=2,5 mm.
$\hat{r}=48$
$\hat{r}=52$
$\hat{r}=56$

Figure 25

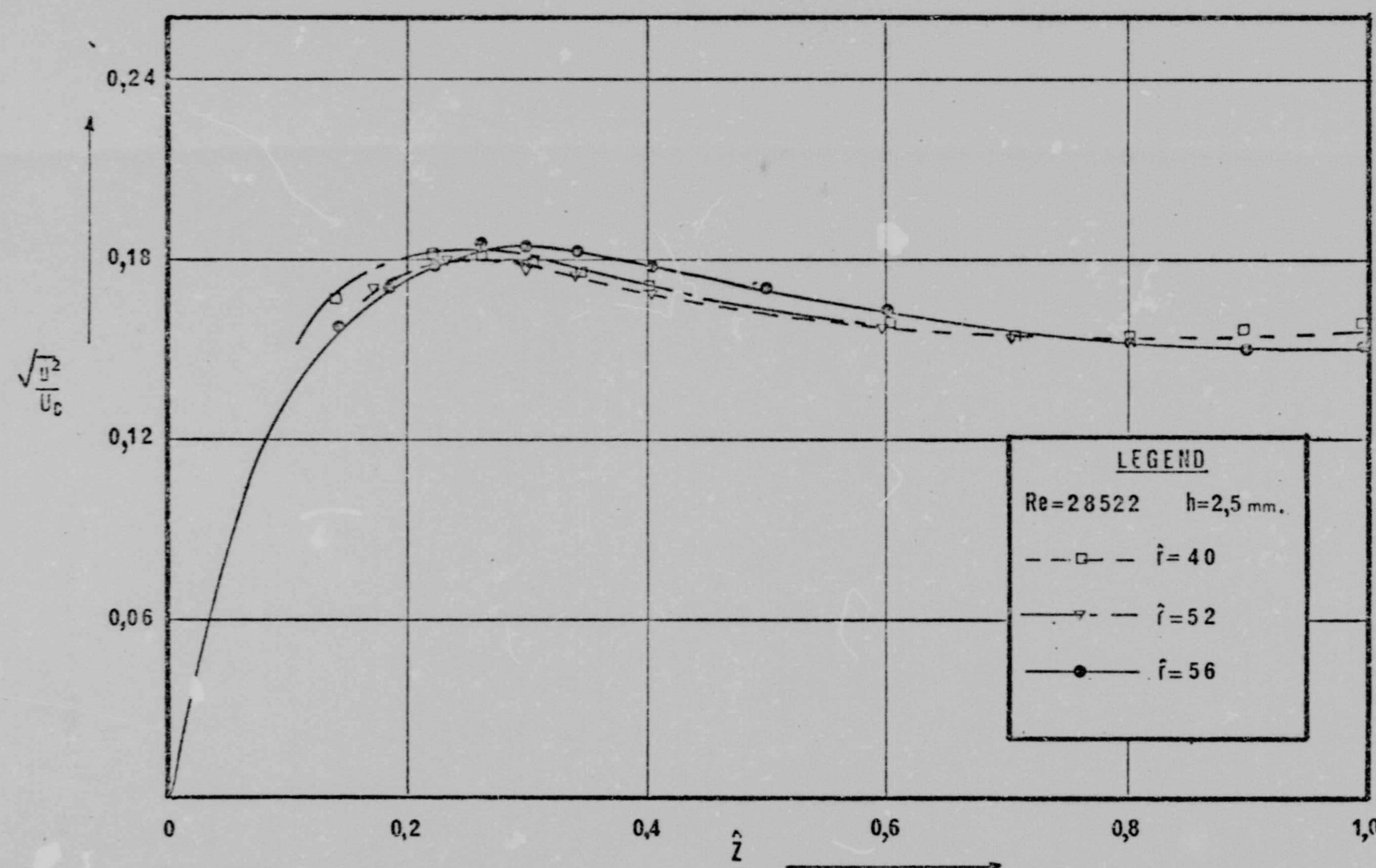
LEGEND
Re=28522 h=2,5 mm.
r̂ = 40
r̂ = 52
r̂ = 56
0,24
0,18
0,12
0,06
0
0,2
0,4
0,6
0,8
1,0
ẑ
$\frac{\sqrt{\overline{u'^2}}}{U_c}$

Figure 26

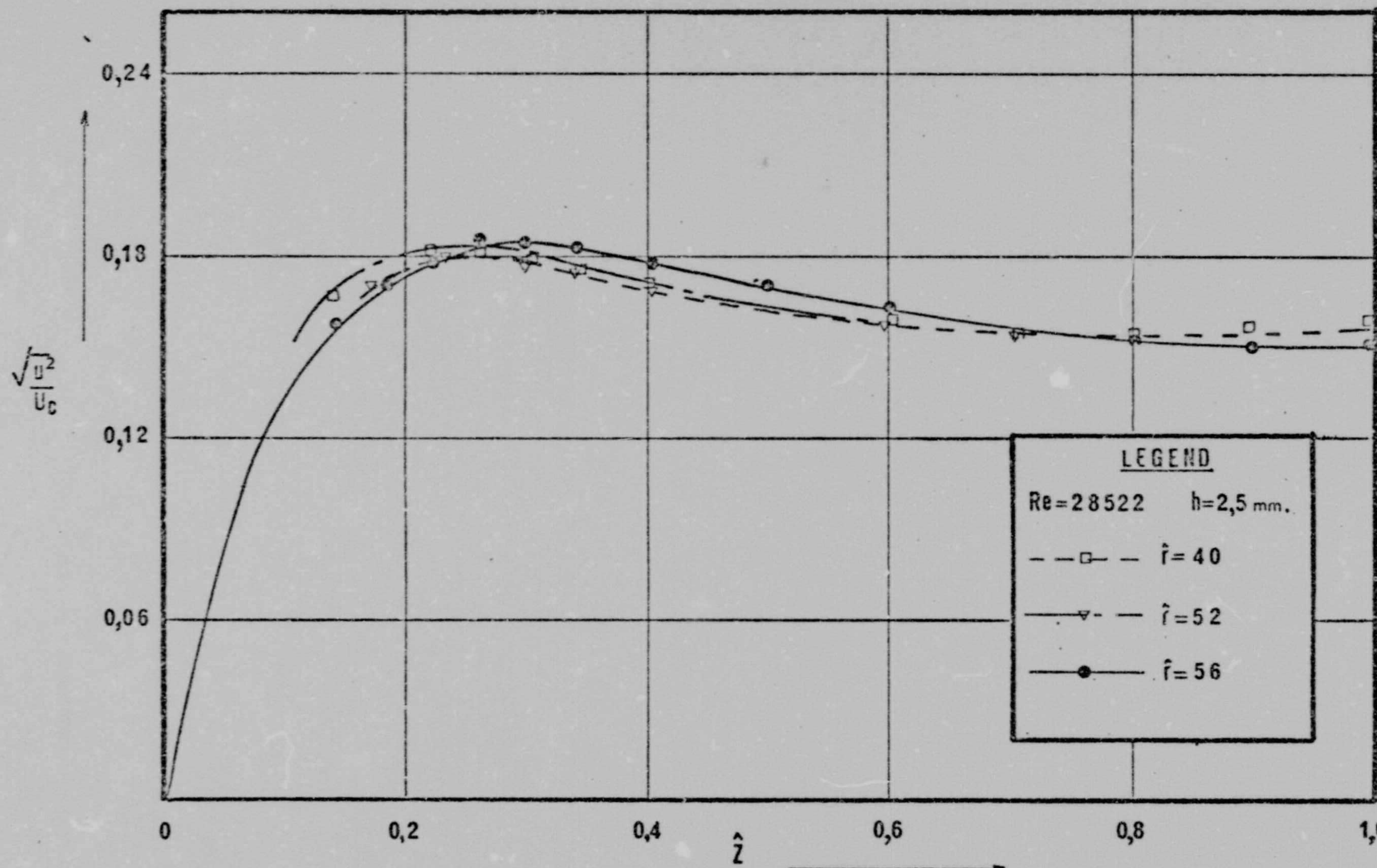
0,24
0,18
0,12
0,06
$\frac{\sqrt{\overline{u'^2}}}{U_c}$
0
0,2
0,4
0,6
0,8
1,0
$\hat{z}$
LEGEND
Re=28522 h=2,5 mm.
$\hat{r}$= 40
$\hat{r}$=52
$\hat{r}$=56

Figure 26

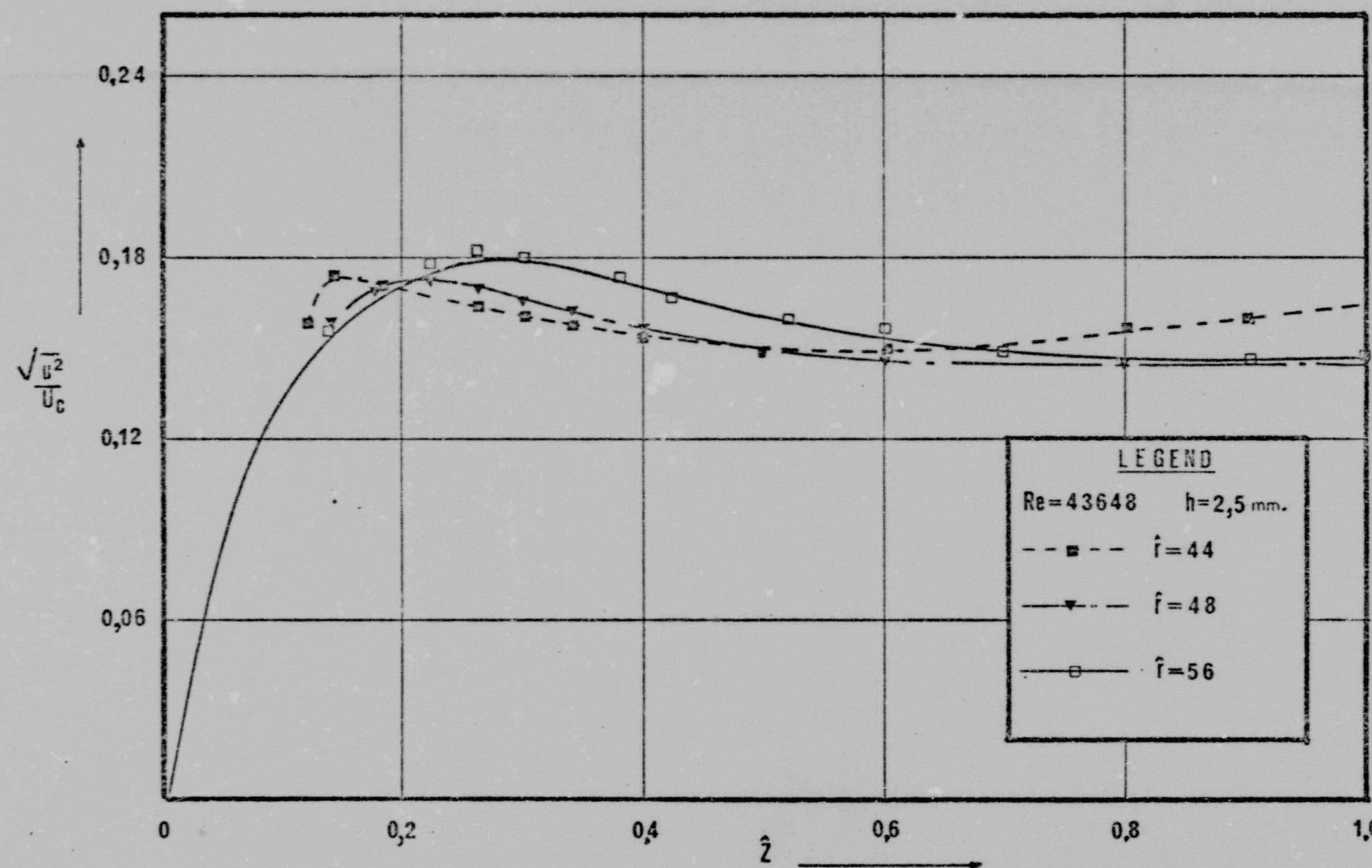
0,24
0,18
0,12
0,06
$\frac{\sqrt{\overline{u'^2}}}{U_c}$
0
0,2
0,4
0,6
0,8
1,0
$\hat{z}$
LEGEND
Re=43648 h=2,5 mm.
$\hat{r}$=44
$\hat{r}$=48
$\hat{r}$=56

Figure 27

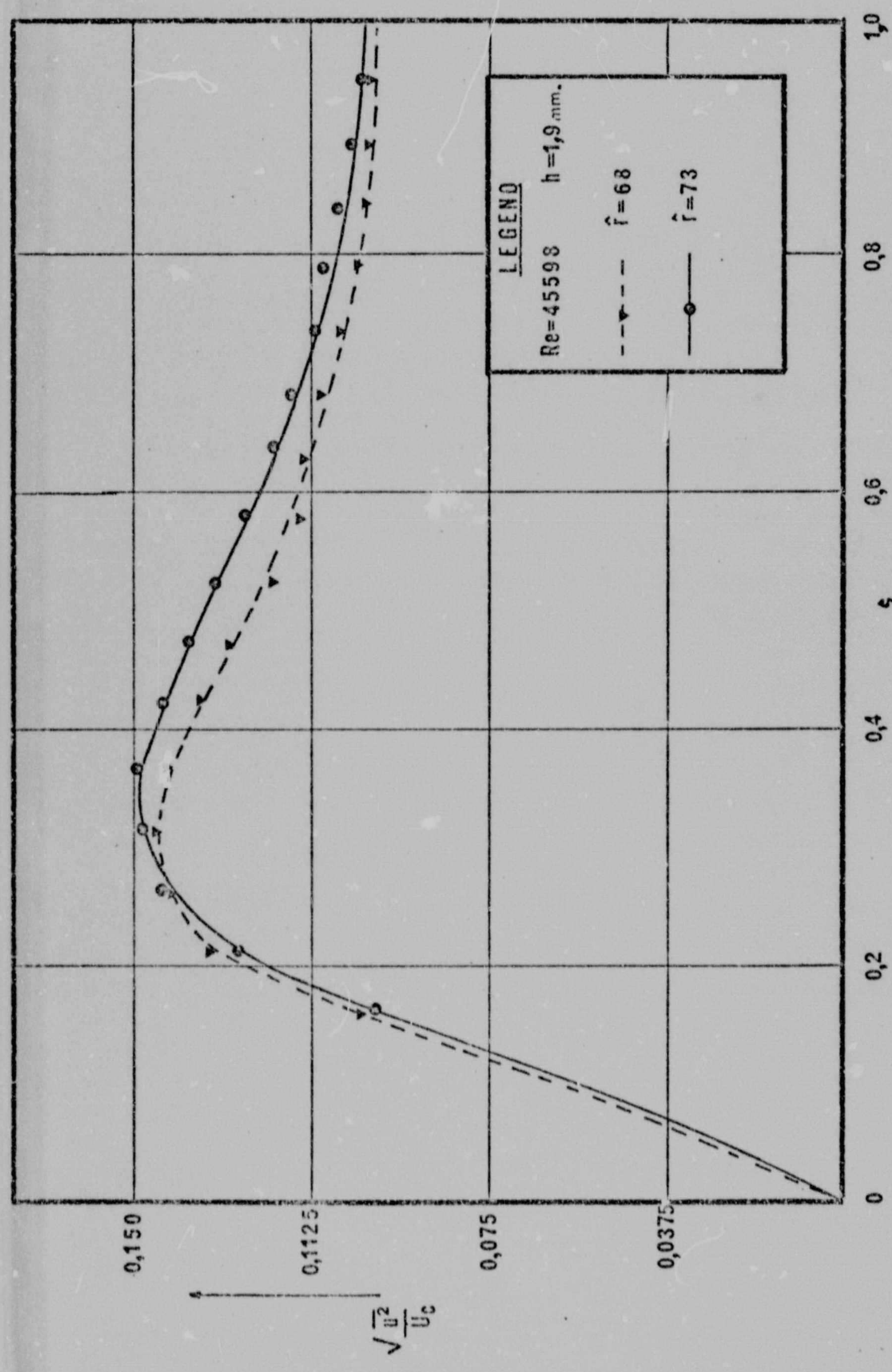
LEGEND
Re=45598
h=1,9 mm.
r̂=68
r̂=73
0,150
0,1125
0,075
0,0375
0
0,2
0,4
0,6
0,8
1,0
ξ

Figure 28